International Journal of Concrete Structures and Materials
Vol.8, No.2, pp.99–116, June 2014
DOI 10.1007/s40069-014-0070-7
ISSN 1976-0485 / eISSN 2234-1315

Effective Length of Reinforced Concrete Columns in Braced Frames

Timo K. Tikka[1),*], and S. Ali Mirza[2)]

(Received March 31, 2013, Accepted January 14, 2014)

Abstract: The American Concrete Institute (ACI) 318-11 permits the use of the moment magnifier method for computing the design ultimate strength of slender reinforced concrete columns that are part of braced frames. This computed strength is influenced by the column effective length factor K, the equivalent uniform bending moment diagram factor C_m and the effective flexural stiffness EI among other factors. For this study, 2,960 simple braced frames subjected to short-term loads were simulated to investigate the effect of using different methods of calculating the effective length factor K when computing the strength of columns in these frames. The theoretically computed column ultimate strengths were compared to the ultimate strengths of the same columns computed from the ACI moment magnifier method using different combinations of equations for K and EI. This study shows that for computing the column ultimate strength, the current practice of using the Jackson–Moreland Alignment Chart is the most accurate method for determining the effective length factor. The study also shows that for computing the column ultimate strength, the accuracy of the moment magnifier method can be further improved by replacing the current ACI equation for EI with a nonlinear equation for EI that includes variables affecting the column stiffness and proposed in an earlier investigation.

Keywords: braced frames, building codes, columns (supports), concrete structures, effective length, reinforced concrete, slenderness, structural design.

List of symbols

A_g, A_{rs}	Area of gross concrete cross section and of longitudinal reinforcing steel bars
C_m	Equivalent uniform bending moment diagram factor
E_c, E_s	Moduli of elasticity of concrete and steel
EI	Effective flexural stiffness of column
e	End eccentricity $= M_2/P_u = M_{col}/P_u$
f'_c	Specified compressive strength of concrete
f_y	Specified yield strength of reinforcing steel bars
G_A, G_B	Relative stiffnesses of column at upper and lower joints
G_{min}	Smaller of G_A and G_B
h, h_{bm}, h_{col}	Overall thickness of cross section of member, beam, and column taken perpendicular to axis of bending
I_g,$I_{g(bm)}$,$I_{g(col)}$	Moment of inertia of gross concrete cross section of member, beam and column
I_{rs}	Moment of inertia of longitudinal reinforcing steel bars taken about centroidal axis of member cross section
K	Effective length factor
ℓ, ℓ_{bm}, ℓ_{col}	Unsupported height (length) of member, beam, and column
M, M_{bm}	Bending moment and beam applied bending moment
M_c	Column design bending moment which includes second-order effects
M_{cs}, M_{col}	Bending moment resistance of cross section and of member (column)
M_{max}	Maximum bending moment acting along column length
M_1, M_2	Smaller and larger of factored moments applied at column ends
M_y, $M_{y(bm)}$	Bending moment acting on member and beam cross section at onset of initial yielding of flexural tension steel computed from ACI Code without using ϕ factors
n	Number of data points
P	Axial load
P_c	Critical axial load strength of column
P_o	Unfactored pure axial load strength of column cross section
P_u	Column axial load strength
$P_{u(des)}$	Column axial load strength computed from one of three design procedures selected for this study

[1)]Stantec Consulting, 200-147 McIntyre Street West, North Bay, ON P1B 2Y5, Canada.
*Corresponding Author; E-mail: timo.tikka@stantec.com
[2)]Professor Emeritus of Civil Engineering, Lakehead University, Thunder Bay, ON P7B 5E1, Canada.

$P_{u(th)}$	Theoretically computed axial load strength of column
r	Radius of gyration of column cross section
β	Dimensionless factor for nonlinear EI equation (Eq. (7))
β_d	Ratio of maximum factored sustained axial load to total factored axial load associated with same load combination
δ_{ns}	Moment magnifier for columns that are part of braced (nonsway) frames
δ_1	Moment magnifier for columns subjected to axial load and equal and opposite end moments causing symmetrical single curvature bending
Δ	Deflection of column due to cord effects
ε_{cu}	Maximum compressive strain in concrete
ρ, ρ_{bm}, ρ_{col}	Total area of longitudinal reinforcing bars divided by gross area of concrete cross section of member, beam, and column
ϕ	Curvature or strength reduction factor
ϕ_k	Stiffness reduction factor

1. Introduction

The strength of a column that is part of a braced frame is influenced by the structural members (beams and columns) framing into the ends of the column. Such a column is subjected to axial load and equal or unequal end moments caused by unbalanced beam loads and deflects laterally between the column ends due to the presence of end moments. The axial load acting through this lateral deflection causes additional (second-order) bending moments along the column height. The second-order bending moments cause additional rotation of the column ends as well as the additional rotation of the members framing into the column. This, in turn, results in changes to the initial bending moments at the ends of the column and to the beam bending moments computed from a conventional elastic frame analysis. The second-order moments caused by the axial load acting through an additional eccentricity (lateral deflection) along the height of a column in a braced frame are less than the second-order moments obtained for an identical isolated column subjected to the same axial load and end moments because of the restraints provided by the beams framing into the column.

ACI 318-11 (2011) permits the use of a moment magnifier approach to approximate the second-order moments due to the axial load acting through the lateral deflection caused by the end moments acting on a column. The moment magnifier approach originated from classical elastic theory and was used for the allowable strength design method of structural steel in the 1960s. This approach was adopted in the United States for the ultimate strength design and in Canada for the limit states design of concrete structures and remains in use today for the design of reinforced concrete slender columns.

In using the moment magnifier method the larger of the column end moments (M_2), computed from a conventional elastic frame analysis, is magnified to include the second-order effects. The axial load (P_u) and magnified column moment (M_c) are then compared to the column cross section axial load-bending moment (P–M) strength interaction diagram and if P_u and M_c fall inside of the cross section interaction diagram, the column meets the strength and slenderness requirements of ACI 318-11. The second-order effects on columns in braced frames are functions of the larger end moment (M_2) in addition to the following parameters: effective length factor (K); effective flexural stiffness of the column (EI); equivalent uniform bending moment diagram factor (C_m); applied axial load (P_u); and sustained load factor (β_d), which is neglected for short-term loads. Earlier studies by the authors documented the examination of the C_m and EI equations available in the literature and proposed a nonlinear but "more accurate" expression for EI (Tikka and Mirza 2004, 2005). The research reported in this paper conducts a similar examination of the available K equations.

The most common procedure used in North America for computing the column effective length factor K is the Jackson–Moreland Alignment Chart, which is easy to use even though it is based on cumbersome equations. Both the Commentary of the ACI 318-11 (2011) and that of the Canadian Standards Association Standard A23.3-04 (CAC 2006) permit the use of this procedure. Duan et al. (1993) proposed a simpler equation for computing the K factor of columns in braced frames. The Commentary of ACI 318-05 (2005) also permitted the use of a set of simple equations for K that were originally developed by Cranston (1972). The accuracy of these equations as related to the effective length factor of columns in braced frames is investigated and discussed in detail in the study reported here.

Almost 3,000 simple reinforced concrete frames in the shape of an inverted T, shown in Fig. 1, were simulated to evaluate the influence of the effective length factor K specified in the Commentary of ACI 318-11 and used in the moment magnifier method for determining the ultimate strength of columns that are part of braced (non-sway) frames subjected to short-term loads. The theoretically computed column ultimate strengths were compared to the ultimate strengths computed from the moment magnifier method using different combinations of equations for K and EI. The columns in these frames were subjected to single or double curvature bending. The beams framing into the columns were subjected to pattern loads causing varying beam bending moments and column end moments. For two load cases, Load Cases 5 and 6 shown in Fig. 1, the top end of the column was also subjected to an applied bending moment. The study concentrates on the examination of equations for the column effective length factor K specified in the Commentary of ACI 318-11 (Jackson–Moreland Alignment Chart) and K proposed by Duan et al. (1993), which are used for computing the column slen-

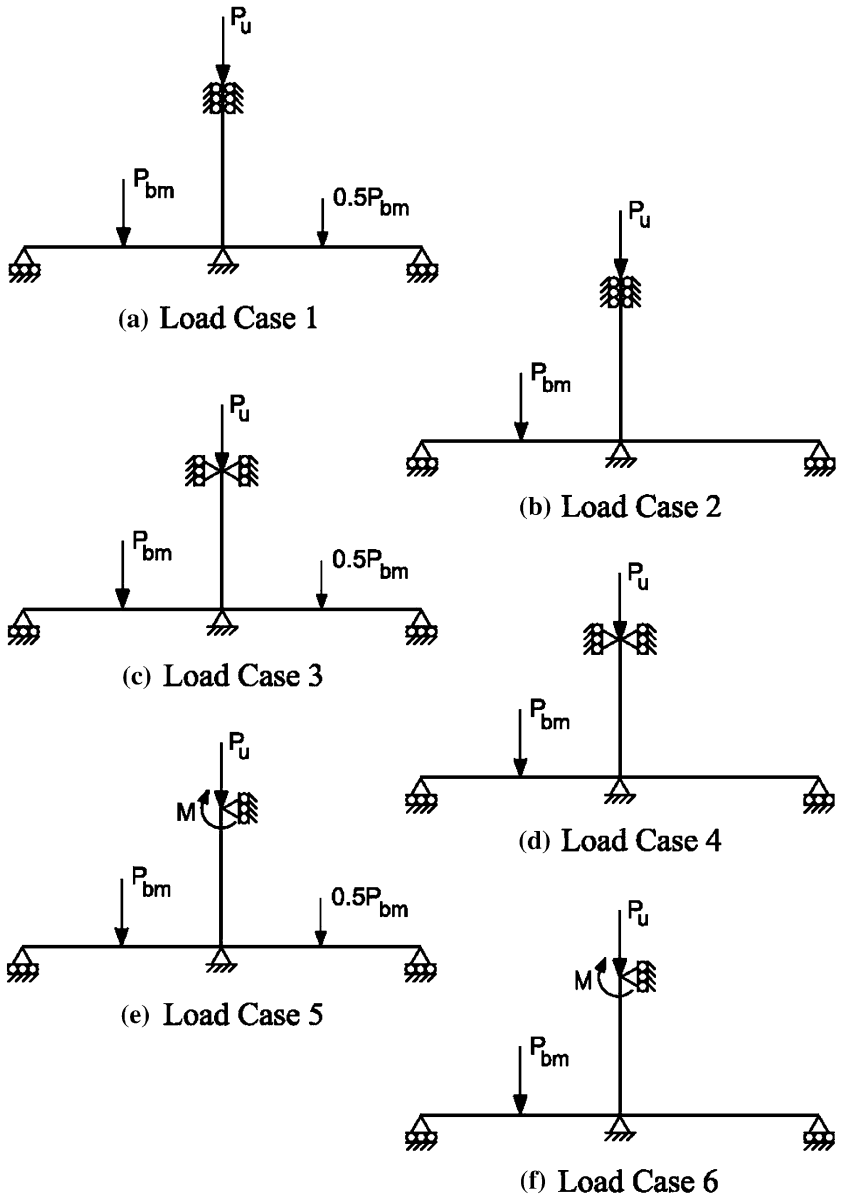

Fig. 1 Frame configurations and load cases used for this study.

derness effect from the ACI moment magnifier approach. These equations for K were examined in combination with those for the column effective flexural stiffness EI specified in ACI 318-11 and EI proposed by Tikka and Mirza (2005).

2. Research Significance

The evaluations of the parameters affecting the moment magnifier method for computing the ultimate strength of slender reinforced concrete columns in braced frames indicate that, of several equations examined for calculating the effective length factor, using the Jackson–Moreland Alignment Chart provides the most accurate results. These evaluations also indicate that the computational accuracy of the moment magnifier method can be further improved if the Jackson–Moreland Alignment Chart for the effective length factor is used along with a nonlinear equation for the column effective flexural stiffness.

3. Development of Theoretical Strength Model

A nonlinear second-order frame analysis procedure was developed to analyze reinforced concrete columns that are part of frames. In order to account for second-order effects due to geometric and material nonlinearities, the theoretical model (computer software) uses: (a) classical stiffness analysis of linear elastic two-dimensional structural frames; (b) iterative technique combined with an incremental method for computing load–deflection behavior and the failure load of the frame; (c) frame discretization to account for the column chord (P–Δ) effects; and (d) P–M–ϕ relationships to account for effects of nonlinear material behavior.

A theoretical cross section strength subroutine was used to compute the P–M–ϕ relationships for a given cross section using force equilibrium and strain compatibility solution. The major assumptions used in determining the P–M–ϕ relationships were: (a) strains between concrete and reinforcing steel were compatible and no slip occurred; (b) the strain was linearly proportional to the distance from the neutral axis; (c) concrete and steel stresses were functions of strains; (d) deflections were small, such that curvatures could be calculated as the second derivative of the deflection; (e) shear stresses were small and their effect on the strength could be neglected; and (f) the confinement of the concrete provided by lateral ties was considered. Further details are documented elsewhere (Tikka and Mirza 2002). Forty-eight P–M–ϕ relationships (axial load levels) were generated and stored for later use to compute the element flexural stiffness.

A reinforced concrete column cross section was assumed to consist of two materials (Fig. 2), concrete and longitudinal reinforcing steel. The concrete was divided into two types, unconfined and partially confined concrete outside and inside the lateral ties, respectively. Therefore, three different stress–strain curves were used to represent the materials in the cross section which was divided into strips and elements as shown in Fig. 2b.

A modified Kent-and-Park (Park et al. 1982) stress–strain relationship, shown in Fig. 2c, was used for concrete in compression. The ascending portion of the curve was described by a second-order parabola and the descending branch of the curve beyond the maximum strength was described by a straight line. The slope of the descending branch for unconfined concrete depended on the concrete strength. For the partially confined concrete, the slope of the descending branch was affected by the concrete strength as well as the level of confinement provided by the lateral ties. The assumed zones of partially confined and unconfined concrete are shown in Fig. 2a. Tension stiffening of concrete was represented by an ascending linear, stress–strain relationship with the maximum tensile strength represented by the modulus of rupture f_r and a linear descending branch (Bazant and Oh, 1984), as shown in Fig. 2c. An elastic–plastic-strain hardening stress–strain relationship, shown in Fig. 2d, was used for the reinforcing steel in tension and compression. In addition, strength reduction due to buckling of longitudinal reinforcing steel in compression was considered in the theoretical procedure, as suggested by Yalcin and Saatcioglu (2000). Further details of the stress–strain curves used for the concrete and reinforcing steel are given in easily available references by Park et al. (1982), Bazant and Oh (1984), and Yalcin and Saatcioglu (2000), and are also documented by Tikka and Mirza (2002), and will not be repeated here.

3.1 Computing Strength of Frames

The frame geometry, cross section properties and prescribed loading configuration were input into the computer

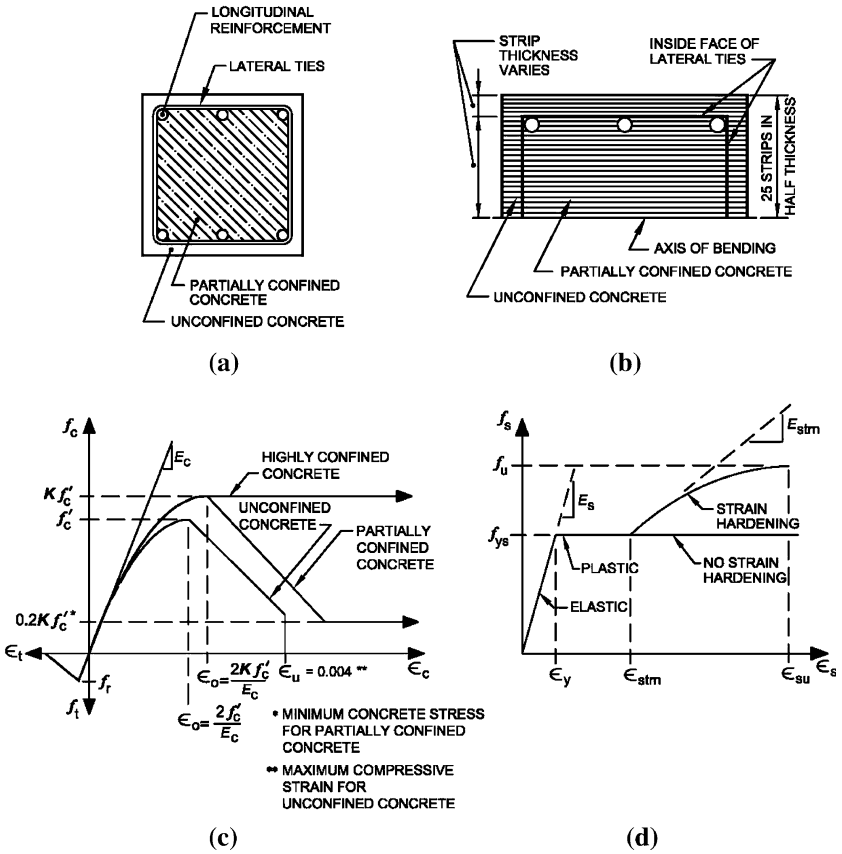

Fig. 2 **a** Details of reinforced concrete cross section used; **b** discretization of one-half reinforced concrete cross section used for computing theoretical strength; **c** schematic concrete stress–strain curves used for computing theoretical strength; and **d** schematic reinforcing steel stress–strain curves used for computing theoretical strength.

program. The frame was discretized into a specified number of elements between nodes (member ends) to permit the frame analysis procedure to account for the second-order member or chord effects (P–Δ) due to axial loads acting through the deformed column(s). The theoretical model permits selected nodal or joint loads to be incremented while other loads are maintained at a constant level. For each increment of loads used for the prescribed loading configuration, the second-order displacements were evaluated using the flexural stiffness of each element and a two-dimensional frame analysis procedure. The element flexural stiffness, for each load increment and displacement iteration, was computed as $EI = M/\phi$ using the basic strength of material concepts applied to members subjected to small deflections. For a given axial load the M–ϕ relationship is known. The loads in the prescribed configuration were incremented until the theoretical failure load was reached. The theoretical failure load was defined as a set of maximum stable forces applied externally to the frame that were in equilibrium with the internal forces within the frame. The beam and column members were discretized into elements equal to the cross section depth.

3.2 Frame Modelling Techniques

Special modelling techniques were used for the frames at beam-to-column joints to account for the additional strength resulting from the concrete confinement at and near the joints, and are similar to those used by Ford, Chang and Breen (1981a, b, c). All of the concrete within the gross cross section at beam-to-column joints was modelled as highly confined and the area of the reinforcing steel in these regions was doubled to account for the confinement provided by additional lap steel and intersection of the members. The concrete within the gross cross section in end portions of a column from the face of the beam to a distance equal to the overall column depth, and in end portions of a beam from the face of the column to a distance equal to the overall beam depth, was modelled as partially confined. The concrete along the remainder of the length of the beams and columns was modelled as unconfined concrete outside the column ties or beam stirrups and partially confined concrete inside the ties/stirrups, as shown in Fig. 3.

The stress–strain relationship for the concrete within the beam-to-column joint, designated as highly confined, was described by an ascending second-order parabola to the peak stress and then maintained as a constant at all strains beyond the strain corresponding to the peak stress (Fig. 2c).

3.3 Experimental Verification of Theoretical Strength Model

The strengths and load–deflection behaviors of 13 braced reinforced concrete test frames were taken from the published literature and used to check the accuracy of the theoretical model. The physical and geometric properties of these frames are shown in Table 1 and Fig. 4 and were taken from Breen and Ferguson (1964), Furlong and Ferguson (1966), and Blomeier and Breen (1975). The frames were constructed with doubly symmetric cross sections using normal-density concrete and subjected to short-term loads. The strength comparisons reported here represent the ultimate tested and computed strengths of frames with no strength reduction factors applied to the computed strengths or computed load–deflection curves.

Comparisons of tested and computed ultimate strengths for the 13 braced frames are given in Table 1 and are plotted in Fig. 5a. Figure 5a also lists the calculated average value, coefficient of variation, minimum value, and maximum value of the tested-to-computed strengths (strength ratios) as 1.02, 0.11, 0.81 and 1.19, respectively, for these frames. The load–deflection curves shown in Fig. 5b, c compare the measured lateral deflections at the mid-height of the column with the theoretically computed lateral deflections for selected test frames. For all other frame tests examined, which are listed in Table 1 but are not shown in Fig. 5b, c, it was found that the shape of the theoretically computed load–deflection curves followed or ran closely parallel to the shape of the measured load–deflection curves. From the strength comparisons, strength ratio statistics and load–deflection curves (Table 1; Fig. 5), it can be seen that the theoretical model, developed in this study, computes the strength of reinforced concrete columns in braced frames with reasonable accuracy.

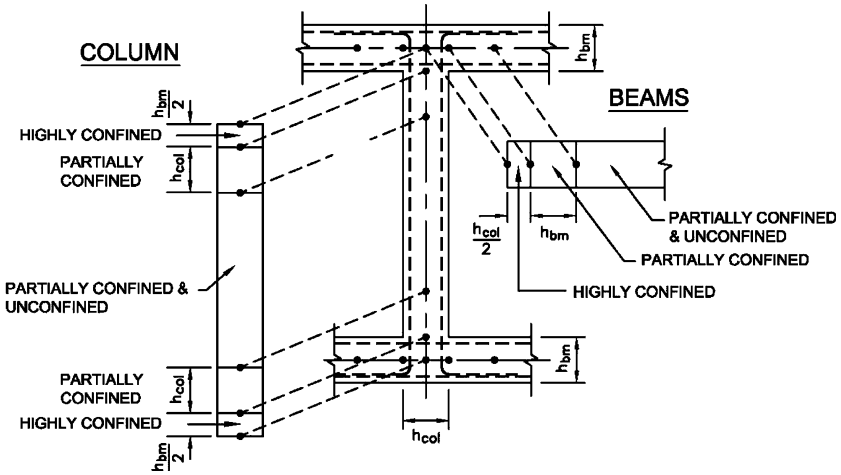

Fig. 3 Regions of concrete confinement used in this study for the theoretical analysis of reinforced concrete test frames.

Table 1 Comparison of tested to theoretically computed strengths of braced frames.

Author	Frame desig.	f'_c (MPa)	Reinf. steel, f_y (MPa)	Reinforcing steel ratio		Slenderness ratio		Col. e/h	Ultimate strength		Tested to computed strength
				ρ_{col}	ρ_{bm}	Col. ℓ/h	Beam ℓ/h		Tested strength (kN)	Computed strength (kN)	
									Axial loads		
Breen and Ferguson (1964)	F1	27.9	349.1	0.017	0.045	30	30	0.300	240.0	220.3	1.090
	F2	21.0	344.8	0.017	0.044	30	30	0.100	262.2	266.9	0.983
	F3	26.7	344.8	0.017	0.041	15	30	0.300	271.1	248.7	1.090
	F4	22.5	344.8	0.017	0.040	15	30	0.100	371.1	344.9	1.076
	F5	25.9	344.8	0.017	0.044	30	30	0.100	320.4	328.2	0.976
									Axial loads		
Furlong and Ferguson (1966)	FF1	23.9	349.7	0.018	0.065	20	17	0.116	266.7	271.3	0.983
	FF2	29.7	378.6	0.018	0.065	20	31	0.106	273.8	316.1	0.866
	FF3	23.0	394.5	0.018	0.065	20	31	0.337	176.4	177.8	0.993
	FF4	22.3	372.4	0.018	0.065	20	17	0.222	233.3	195.6	1.193
	FF5	22.3	364.1	0.018	0.065	15	37	0.097	246.7	302.9	0.814
	FF6	24.5	349.0	0.018	0.065	15	37	0.320	202.2	201.6	1.003
									Axial loads		
Blomeier and Breen (1975)	B2	62.8	385.5	0.012	0.038	15	26	0.100	534.7	537.3	0.995
	B3	38.7	381.4	0.012	0.038	15	26	0.100	443.6	374.0	1.186

Note For 13 braced frame tests, average strength ratio = 1.02, coefficient of variation = 0.11.

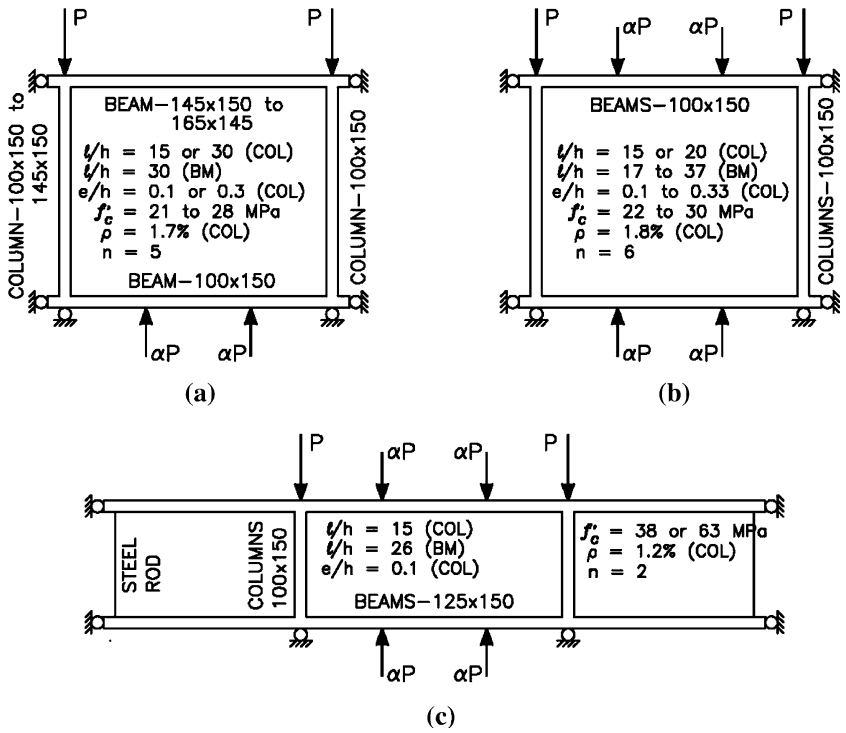

Fig. 4 Configurations of braced reinforced concrete test frames: **a** Breen and Ferguson (1964); **b** Furlong and Ferguson (1966); and **c** Blomeier and Breen (1975).

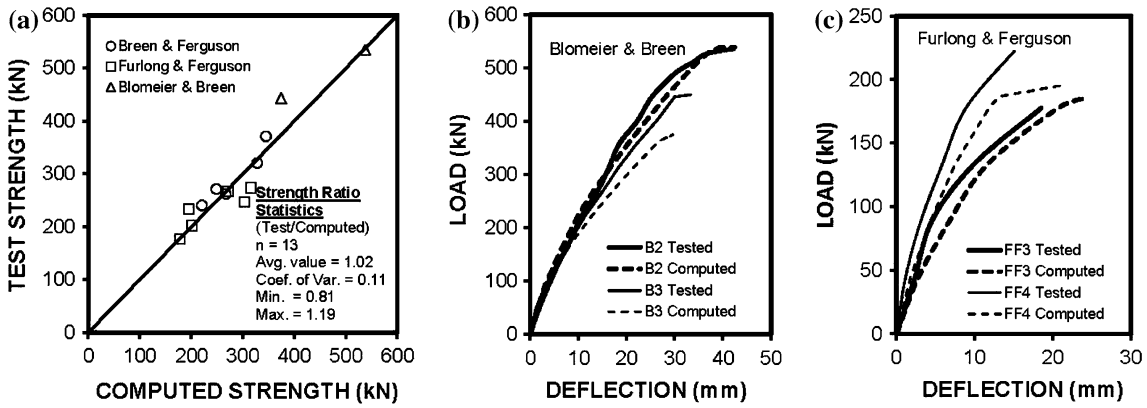

Fig. 5 Comparison of tested to theoretically computed values for braced reinforced concrete frames: **a** comparison of strengths; and **b** and **c** comparison of load–deflection curves measured and computed at mid-height of the column.

4. Description of Simulated Reinforced Concrete Braced Frames

For the analysis of simulated reinforced concrete braced frames used in this study, the cross section properties of the columns and beams were kept constant. The lower end of a column having a gross cross section of 305 mm × 305 mm (Fig. 6a) was framed rigidly into two beams of equal spans having a cross section of 305 mm wide by 610 mm deep (Fig. 6b). Previous studies have concluded that a smaller cross section size was more critical for investigating the strength and flexural stiffness of slender reinforced concrete columns (Mirza and MacGregor 1989; Mirza 1990). Hence, the overall dimensions of 305 mm × 305 mm were chosen for the column cross section. Similarly, the column longitudinal reinforcing steel ratio (ρ_{col}) in simulated frames was kept constant at about 2 %, which is within the lower one-third of the usual range of 1–4 % for ρ_{col} (Mirza 1990). Note that concrete columns with light longitudinal reinforcing are more critical for investigating strength ratios (Mirza and MacGregor 1989). The strength of a column in a braced frame is partly a function of the stiffness of the column relative to the stiffnesses of the other members framing into upper and lower joints of the column. In this study, the relative stiffness of the column was varied by varying the column and beam lengths. The column and beam sizes and ρ_{col} selected are representative of members that would be expected in lowrise buildings. The nominal compressive strength of concrete (f'_c) and yield strength of reinforcing steel (f_y) were taken as 34.5 MPa and 414 MPa, respectively. Again, these values of f'_c and f_y were selected because they are most commonly used in building construction and also because a previous study showed that f'_c of 34.5 MPa can be used to conservatively estimate the strength ratios of slender columns having lower concrete strengths (Mirza and MacGregor 1989).

The variables studied to examine the effective length factor used in the ACI 318-11 moment magnifier approach for columns in reinforced concrete braced frames are as follows: (a) The load patterns, the end conditions at the top

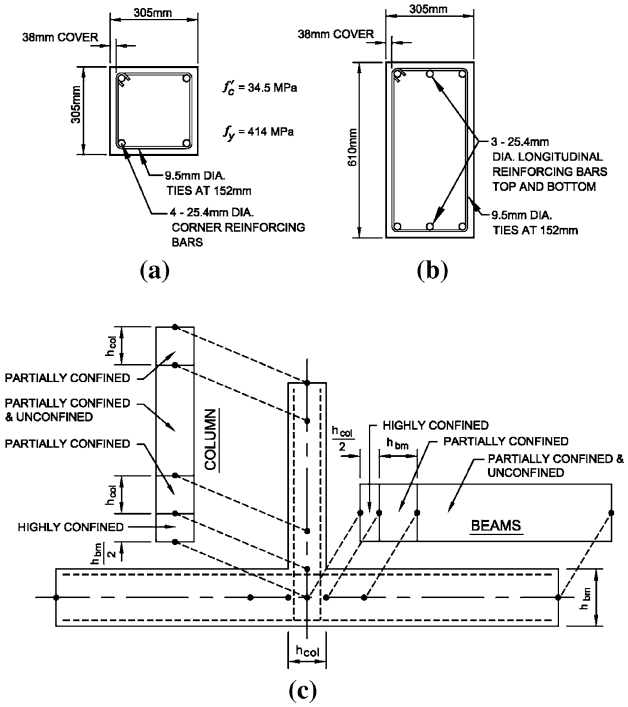

Fig. 6 Member properties used in this study for the theoretical analysis of simulated reinforced concrete frames: **a** column cross section; **b** beam cross section; and **c** regions of concrete confinement.

of the column (fix-ended or pin-ended), and the end moment applied to the upper end of the column (when pin-ended) producing 6 different load cases (Fig. 1); (b) the slenderness ratio of the column (ℓ_{col}/h_{col}), where ℓ_{col} = unsupported height of the column, h_{col} = overall thickness of the column cross section; (c) the slenderness ratio of the beams (ℓ_{bm}/h_{bm}), where ℓ_{bm} = unsupported length of the beam, h_{bm} = overall thickness of the beam cross section; and (d) the magnitude of the beam loading controlled by the ratio of the beam applied bending moment to the yield bending moment ($M_{bm}/M_{y(bm)}$), where the yield bending moment is defined as the bending moment acting on the beam cross section at the onset of initial yielding of the beam flexural tension steel and computed from the ACI Code without

using the ϕ factors. Specified values of variables used for this study are given in Table 2. Note that the variation in column and beam slenderness ratios and the column upper end conditions (pin-ended or fix-ended) produced a range of effective lengths that permitted the evaluation of the effective length factor (K). Some combinations of the column and beam slenderness ratios listed in Table 2 produced impractical frames. However, all simulated columns for which theoretically-computed δ_{ns} values were greater than 1.0 were included in the analysis. This permitted the examination of higher ranges of relative column stiffnesses and the resulting K factors than would have been otherwise possible. Table 2 also indicates that the magnitude of the beam loads shown in Fig. 1 was varied in order to study the effect of yielding of the flexural tension reinforcing steel in the beams. Figure 1 shows schematically how the loads were applied to the beams. These beam loads were applied so that the maximum computed bending moment in one of the beams was equal to the predefined moment that ranged from 0.84 $M_{y(bm)}$ to 1.12 $M_{y(bm)}$ (Table 2), representing conditions at or near ultimate loads. Note that the ratio of the ultimate moment to yield moment for the beam cross section, shown in Fig. 6b, was computed from the ACI Code (without ϕ factors) as 1.12.

The 2,960 frames described by specified cross section properties, material strengths, and loading conditions shown in Table 2 and Fig. 1 were simulated. The computed strengths of columns in these frames were then used to examine and evaluate the effective length factor.

5. Theoretical Procedure Used for Computing Ultimate Strength of Columns in Simulated Braced Frames

The first step in computing the theoretical ultimate strength of a column was to compute the first-order bending moments acting at the column ends (M_1 and M_2) resulting from the applied beam loads and, for load cases 5 and 6 (Fig. 1), also resulting from the applied column end moment. For computing the first-order bending moments from a conventional elastic analysis, the column and beam stiffnesses were computed as 0.7 $E_cI_{g(col)}$ and 0.35 $E_cI_{g(bm)}$, respectively, where E_c = modulus of elasticity of concrete, and $I_{g(col)}$, $I_{g(bm)}$ = moments of inertia of the column and beam gross cross sections, respectively. The bending moments along the length of the beams were checked to ensure that the beam bending moment ratio ($M_{bm}/M_{y(bm)}$) was at the predefined level (Table 2). If the beam bending moments did not correspond to the desired beam bending moment ratio, the beam loads were multiplied by a scale factor to bring them to the desired level.

To determine the theoretical axial load strength ($P_{u(th)}$) of a column, the axial load was incremented to failure starting from an axial load equal to 10 % of the concentric axial load strength of the column cross section. The theoretical strength model described in an earlier section was used for this purpose.

For load cases 5 and 6 (Fig. 1), the moment at the top end of the column was applied proportionally to the axial load to

Table 2 Specified properties of simulated reinforced concrete frames.

Load case	Properties	Specified values	Number of specified values
1 and 2 Upper end of column fixed against rotation, as shown in Fig. 1a and b	ℓ_{col}/h_{col}	15; 17.5; 20; 22.5; 25; 27.5; 30; 32.5;35; 37.5; 40; 42.5; 45; 47.5;50; 52.5; 55	17
	ℓ_{bm}/h_{bm}	10; 15; 20; 30; 40	5
	$M_{bm}/M_{y(bm)}$	0.84; 1.00; 1.06; 1.12	4
	Total number of simulated frames equals (17 × 5 × 4 =) 340 for Load Case 1 and 340 for Load Case 2		
3 and 4 Upper end of column pin-ended, as shown in Fig. 1c and d	ℓ_{col}/h_{col}	10; 12.5; 15; 17.5; 20; 22.5; 25; 27.5; 30; 32.5; 35; 37.5; 40; 42.5; 45	15
	ℓ_{bm}/h_{bm}	10; 15; 20; 30; 40	5
	$M_{bm}/M_{y(bm)}$	0.84; 1.00; 1.06; 1.12	4
	Total number of simulated frames equals (15 × 5 × 4 =) 300 for load case 3 and 300 for Load Case 4		
5 and 6 Bending moment applied to upper end of column which is pin-ended, as shown in Fig. 1e and f	ℓ_{col}/h_{col}	15; 20; 25; 30; 35; 40	6
	ℓ_{bm}/h_{bm}	10; 15; 20; 30; 40	5
	$M_{bm}/M_{y(bm)}$	0.84; 1.00; 1.06; 1.12	4
	$M/(P_u\ h)$	0.1; 0.2; 0.3; 0.4; 0.6; 0.8; 1.0	7
	Total number of simulated frames equals (6 × 5 × 4 × 7 =) 840 for load case 5 and 840 for load case 6		

Note Each simulated frame had a different combination of specified properties shown above with f'_c = 34.5 MPa and f_y = 414 MPa

maintain the predefined end eccentricity that corresponded to one of the M/P_uh values given in Table 2. Therefore, the applied bending moment at the top end of the column increased at the same rate as the axial load. Since at each iteration of the axial load the bending moment at the top end of the column changed, a new first-order elastic analysis was performed and the beam loads were adjusted to maintain the beam bending moment ratio($M_{bm}/M_{y(bm)}$). The nonlinear second-order analysis was then used to compute the maximum bending moment along the column length for the axial load under consideration. The second-order bending moments in the beams were also monitored to ensure that the failure of the column took place prior to the failure of a beam. If the failure of one of the beams occurred before the column failure, the beam loads were adjusted and the entire process was repeated.

The computed column end moments and the maximum moment in the column from both the first-order elastic analysis and the second-order analysis were stored. The first-order end moment ratio (M_1/M_2) and end eccentricity ratio ($e/h = M_2/hP_{u(th)}$) were also computed and stored along with $P_{u(th)}$ for the column in the frame under consideration and were used in analyses presented in the later part of this paper. Note that, for load cases 1–4 (Fig. 1), M_2 was equal to the unbalanced beam moment at the bottom end of the column, whereas M_1 was located at the top end of the column. For these load cases, M_1/M_2 ratio was equal to -0.5 for load cases 1 and 2 (fix-ended) and zero for load cases 3 and 4 (pin-ended). For load cases 5 and 6 (Fig. 1), the top end of the column was subjected to a predefined applied bending moment that corresponded to an applied end eccentricity ratio M/P_uh given in Table 2, and the bottom end of the column was subjected to the unbalanced beam moment. For these load cases, M_2 was located at the top end of the column and the M_1/M_2 ratio ranged from approximately -0.4 to almost 1.0. Hence, the M_1/M_2 ratio for columns in frames used in this study varied from -0.5 to 1.0.

Special techniques discussed in an earlier section of this paper were used for modeling beam-to-column joints in frames to account for the additional strength resulting from confinement effects. As shown in Fig. 6c, concrete within the gross cross section at the beam-to-column joint was modeled as highly confined and the area of the reinforcing steel in this region was doubled for the purpose of modeling. The concrete within the gross cross section in end portions of the column (from the face of the beam or from the top of the column to a distance equal to the overall column depth) and in end portions of beams (from the face of the column to a distance equal to the overall beam depth) was modeled as partially confined. The remaining parts of frames were modeled with unconfined concrete outside column ties/beam stirrups and partially confined concrete inside column ties/beam stirrups. The stress–strain curves given in Fig. 2c were used to define highly confined, partially confined, and unconfined concretes.

6. Design Procedures Used for Computing Ultimate Strength of Columns in Simulated Braced Frames

6.1 ACI 318-11 Moment Magnifier Method

The procedure described in this section was used to compute the slender column strength from the ACI moment magnifier approach. Note that the strength and stiffness reduction factors (ϕ and ϕ_k for ACI) were taken equal to 1.0 in this study.

The first step in computing the ACI ultimate strength of a slender column that is part of a braced frame is to determine the cross section strength, which is represented by an axial load-bending moment (P–M) strength interaction diagram, similar to the one shown in Fig. 7. The cross section strength interaction diagram was defined by 102 points that were computed using the compatibility of strains and the equilibrium of forces acting on the cross section. For computing the ACI cross section strength, it was assumed that (a) the strains are linearly proportional to the distances from the neutral axis; (b) the maximum concrete strain $\varepsilon_{cu} = 0.003$ exists at the extreme compression fiber as given in ACI 318-11; (c) the compressive stress in concrete is represented by a rectangular stress block as defined in ACI 318-11; (d) the specified concrete strength is used in computing the maximum concrete stress in the stress block; and (e) the concrete is assumed to have no strength in tension.

To develop the points on the cross section strength interaction diagram, the strain at the extreme compression fiber was held constant at $\varepsilon_{cu} = 0.003$, while the strain at the extreme fiber on the opposite face was incremented from a strain that equaled the maximum computed tensile strain at pure bending up to a strain that was equal to the uniform

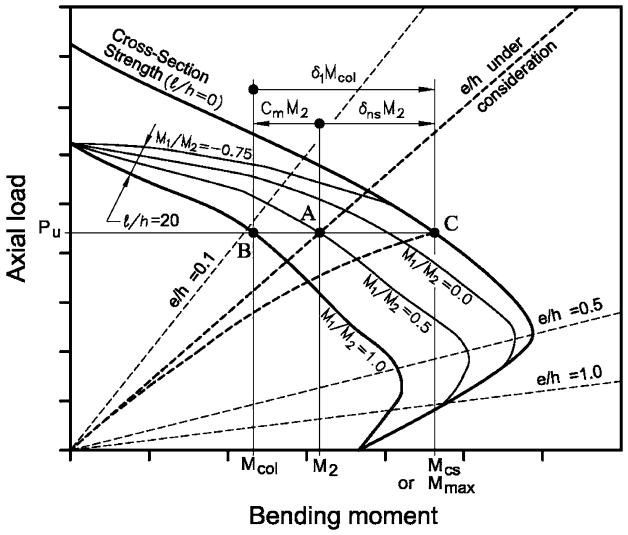

Fig. 7 Schematic cross section and column (member) ultimate axial load-bending moment interaction diagrams for an isolated column.

compressive strain required across the entire cross section for pure compression. The summation of forces acting on concrete and reinforcing steel at each increment of strain generated one point on the cross section axial force-bending moment interaction diagram. The entire interaction diagram for a column cross section ($\ell/h = 0$) similar to one shown in Fig. 7 was defined by 102 points, as stated earlier.

The ACI moment magnifier procedure for slender columns uses the moment magnifier δ_{ns} and the larger of the two column end moments M_2 obtained from a conventional elastic frame analysis to compute the magnified moment M_c (M_{max}), which includes second-order effects occurring along the height of the column:

$$M_{max} = M_c = \delta_{ns} M_2 = C_m \delta_1 M_2 \geq M_2 \tag{1}$$

In Eq. (1), δ_{ns} is the moment magnifier for columns that are part of braced (nonsway) frames; M_2 is the larger of the two factored end moments (M_1 and M_2) computed from a conventional elastic frame analysis and is always taken as positive; C_m is the equivalent uniform moment diagram factor; and δ_1 is the moment magnifier for the same columns when subjected to axial load and equal and opposite (equivalent) end moments causing symmetrical single curvature bending. Chen and Lui (1987) explain that the C_m and δ_1 for pin-ended columns subjected to end moments can be derived from the basic differential equation governing the elastic in-plane behavior of a column. For design purposes, ACI has adopted a simplified and widely accepted approximation of δ_{ns}:

$$\delta_{ns} = C_m \delta_1 = \frac{0.6 + 0.4 M_1/M_2}{1 - \frac{P_u}{\phi_k P_c}} \geq 1.0 \tag{2}$$

In Eq. (2), P_u is the applied axial load under consideration; ϕ_k is the stiffness reduction factor specified as 0.75 in ACI 318-11 but taken as 1.0 for this study; and P_c is the critical buckling load computed from

$$P_c = \frac{\pi^2 EI}{(K\ell)^2} \tag{3}$$

In Eq. (3), ℓ is the column length; K is the effective length factor; and EI is the effective flexural stiffness. For computing the effective flexural stiffness (EI) of tied slender reinforced concrete columns for short-term loads ($\beta_d = 0$), the ACI Code permits the use of Eq. (4):

$$EI = 0.2 E_c I_g + E_s I_{rs} \tag{4}$$

where I_{rs} = moment of inertia of the longitudinal reinforcing bars taken about the centroidal axis of the column cross section. The commentary of ACI 318-11 (2011) permits the use of the Jackson–Moreland Alignment Chart, which is based on Eq. (5), for determining the effective length factor K for columns in braced frames:

$$\frac{G_A G_B}{4}\left(\frac{\pi}{K}\right)^2 + \left(\frac{G_A + G_B}{2}\right)\left(1 - \frac{\pi/K}{\tan(\pi/K)}\right) + \frac{2\tan(\pi/2K)}{(\pi/K)} - 1 = 0 \tag{5}$$

In Eq. (5), G_A and G_B are the relative stiffnesses of the column at upper and lower joints, respectively, and were computed as the ratios of the sum of stiffnesses of columns ($\sum(EI/\ell)_{col}$) meeting at the joint A or B to the sum of stiffnesses of beams ($\sum(EI/\ell)_{bm}$) meeting at the same joint. A graphical representation of Eq. (5) (Jackson–Moreland Alignment Chart) is given in Fig. 8, which shows the range of K examined in this study.

For G_A and G_B, EI values were computed from $0.7E_cI_{g(col)}$ and $0.35E_cI_{g(bm)}$ for columns and beams, respectively, as permitted by the ACI Code. For frames used in this study (Fig. 1), the upper end of the column (Joint A) has no beams framing into it. The upper end of the column is either pin-ended or fix-ended and, therefore, G_A is theoretically infinity or zero, respectively. To avoid numerical problems in solving Eq. (5), G_A was set equal to 1,000 when the upper end of the column was pin-ended and taken as 0.001 when the upper end of the column was fix-ended.

Equation (1) can be used to obtain the bending moment resistance of a column in a frame for a given level of axial load (P_u) directly from the cross section strength interaction diagram. To do this, the cross section bending moment

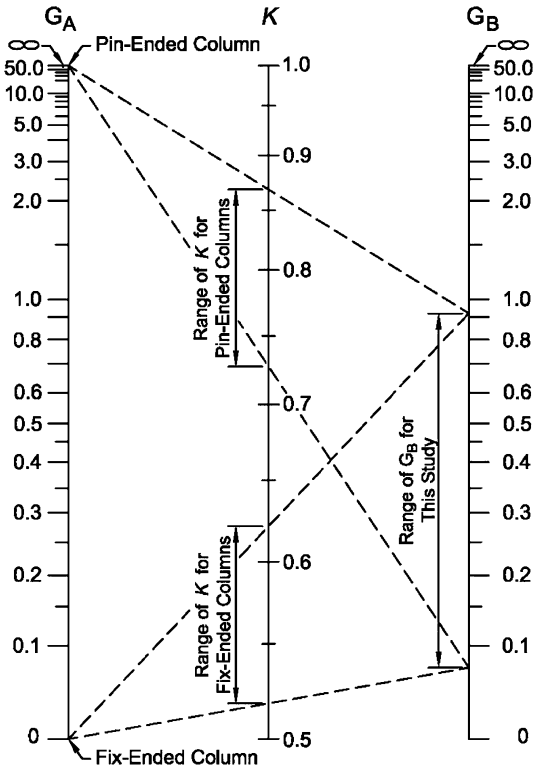

Fig. 8 Jackson–Moreland Alignment Chart for braced frames showing the range of effective length factor examined in this study.

resistance (M_{cs}) is substituted for the magnified column moment (M_c) in Eq. (1). Then, the larger of the two end moments (M_2), which can be applied to the column at the given axial load $P_{u,}$ is computed by solving Eq. (1) for M_2:

$$M_2 = \frac{M_{cs}}{\delta_{ns}} \tag{6}$$

To generate the column axial load-bending moment interaction diagram (Fig. 7), the cross section bending moment resistance M_{cs} for each level of axial load (P_u) was divided by δ_{ns}. Note that the maximum axial load that can be applied to a slender column is less than the pure axial load resistance of the cross section (P_o) and is also less than the column critical load resistance (P_c) computed from Eq. (3). Hence, the points on the column strength interaction curve were generated for P_u values that were lower than both P_o and P_c. Note that, for reinforced concrete columns examined in this study, P_o was computed from $0.8[(0.85f_c')(A_g - A_{rs}) + f_y A_{rs}]$, as permitted by ACI 318-11 (2011), where f_c', f_y = specified compressive and yield strengths of concrete and reinforcing steel, and A_g, A_{rs} = areas of the gross concrete cross section and of the longitudinal reinforcing steel.

For an M_1/M_2 ratio, M_2 values were computed from the procedure described above for all levels of axial load (P_u) that were lower than or equal to both P_o and P_c. This generated the column axial load-bending moment interaction diagram for the M_1/M_2 ratio under consideration. Repeating the step for all desired M_1/M_2 ratios generated a series of column strength interaction curves. Four of such curves for $M_1/M_2 = 1.0$, 0.5, 0.0 and -0.75 are shown in Fig. 7. The ACI axial load strength ($P_{u(des)}$) of a column was then computed from linear interpolation of points on these interaction diagrams, using the first order M_1/M_2 and e/h ratios determined earlier for that column from the theoretical procedure described in the preceding section.

6.2 Modified ACI Moment Magnifier Method with Alternative (Nonlinear) *EI* Equation

The procedure outlined above is applicable only when *EI* is computed from the ACI *EI* equation (Eq. (4)) or from a similar *EI* equation used for calculating P_c from Eq. (3). This is because the ACI *EI* from Eq. (4) remains constant regardless of the magnitude of end moments and, therefore, P_c also remains constant. As a result, the moment magnifier (δ_{ns}) remains constant for a given column. However, P_c is strongly influenced by the effective flexural stiffness (*EI*), which varies due to the nonlinearity of the concrete stress–strain curve and cracking along the height of the column among other factors. Based on extensive analyses of 11,550 simulated and 128 physically-tested reinforced concrete columns, Tikka and Mirza (2005) proposed an *EI* design equation for short term loads, reproduced here as Eq. (7), that is dependent upon the end eccentricity ratio (e/h), making *EI* both variable and nonlinear:

$$EI = \left(0.47 - 3.5\frac{e}{h}\left(\frac{1}{1+\beta\frac{e}{h}}\right) + 0.003\frac{\ell}{h}\right)E_c I_g + 0.8E_s I_{rs} \tag{7}$$

where $\beta = 7.0$ for columns with $\rho_{col} \le 2$ %; and $\beta = 8.0$ for columns with $\rho_{col} > 2$ %. For developing Eq. (7), Tikka and Mirza (2005) examined the practical ranges of a number of variables that could possibly affect the effective flexural stiffness of reinforced concrete columns. They found that the column e/h, ℓ/h and ρ_{col} had major, significant, and minor effects, respectively, on the column *EI* and, hence, included these variables in Eq. (7). The variable and nonlinear nature of Eq. (7) affects P_c which, in turn, affects δ_{ns}. Therefore, an iterative approach was used to determine the slender column strength interaction diagram when Eq. (7) was used in lieu of Eq. (4) for *EI* in the moment magnifier procedure.

The smaller of the cross section pure axial load strength (P_o) and the column critical load strength (P_c) was used to establish the upper limit for the axial load levels to be used in determining the slender column strength interaction diagram. For each level of axial load (P_u), the end eccentricity (e) was iterated until $e \times P_u \times \delta_{ns} = M_{cs}$ was satisfied within a tolerance of 0.01 %. The moment magnifier (δ_{ns}) was computed from Eq. (2) for a given M_1/M_2 ratio for each iteration of end eccentricity using the *EI* computed from Eq. (7) and the effective length factor (K) computed from Eq. (5). This generated one point on the column strength interaction curve for the M_1/M_2 ratio under consideration. Repeating this step for all axial load levels generated the entire strength interaction curve for the M_1/M_2 ratio under consideration. Such column strength interaction diagrams were generated for a series of M_1/M_2 ratios and were used for computing the modified ACI axial load strength ($P_{u(des)}$) of a column from linear interpolation, using the first-order M_1/M_2 and e/h ratios calculated for that column from the theoretical procedure described in an earlier section.

6.3 Modified ACI Moment Magnifier Method with Alternative (Simplified) Equation for *K* Factor

A simple equation for the effective length factor was proposed by Duan et al. (1993) for columns in nonsway frames:

$$K = 1 - \frac{1}{5 + 9G_A} - \frac{1}{5 + 9G_B} - \frac{1}{10 + G_A G_B} \tag{8}$$

In addition, the Commentary to ACI 318-05 (2005) permitted the use of expressions proposed by Cranston (1972), where K was taken as the smaller of the following for columns in nonsway frames:

$$K = 0.7 + 0.05(G_A + G_B) \le 1.0 \tag{9a}$$

$$K = 0.85 + 0.05G_{\min} \le 1.0 \tag{9b}$$

in which $G_{\min}$ was the smaller of G_A and G_B. A comparison of K computed from Eq. (5) (Jackson–Moreland Alignment

Chart), Eq. (8) (Duan et al. 1993) and Eq. (9) (Cranston 1972) is shown in Fig. 9. The following observations can be made from Fig. 9: (a) Cranston's expressions produce effective length factors that are very conservative compared to the values obtained from the Jackson–Moreland Alignment Chart when the upper joint is fix-ended ($G_A = 0$); (b) Duan's equation produces effective length factors that are almost the same as those obtained from the Jackson–Moreland Alignment Chart when the upper joint is fix-ended ($G_A = 0$); and (c) when the upper joint is pin-ended ($G_A = \infty$), both Duan's and Cranston's equations produce conservative results compared to the effective length factor computed from the Jackson–Moreland Alignment Chart.

To investigate the effect of the K factor computed from Duan et al. (1993) on the strength of slender reinforced concrete columns, Eq. (8) was used in place of Eq. (5) and the rest of one of the two moment magnifier procedures described previously was followed, depending on whether the ACI equation (Eq. (4)) or the alternative equation (Eq. (7)) was used for calculating EI. No further analysis was performed with Cranston's equation (1972), because it produced very conservative values of K for fix-ended columns in Fig. 9a and similar values of K as those produced by the Duan et al. equation for pin-ended columns in Fig. 9b.

7. Computation of Ultimate Strength of Columns in Simulated Braced Frames

To evaluate the effective length factor used in the moment magnifier approach for determining column strength, 2,960 simple reinforced concrete frames were simulated. The cross section and material properties of columns and beams used in these frames are shown in Fig. 6. The combinations of support conditions and applied loads produced six different load cases (Fig. 1). Each frame had a different combination of column slenderness ratio, beam slenderness ratio, support condition, and beam loads (Table 2). The column theoretical ultimate strengths ($P_{u(th)}$) were computed from the procedure outlined in a previous section. The column design ultimate strengths $P_{u(des)}$ were calculated from the design procedures described in the preceding section using several combinations of (a) Eq. (5) (Jackson–Moreland Alignment Chart) or Eq. (8) (Duan et al. 1993) for computing the effective length factor K; and (b) Eq. (4) (ACI) or Eq. (7) (Tikka and Mirza 2005) for the column effective flexural stiffness EI used in the computation of P_c. Note that ϕ and ϕ_k factors were taken equal to 1.0 for computing $P_{u(des)}$. Finally, the strength ratios were computed by dividing $P_{u(th)}$ by $P_{u(des)}$, which were statistically analyzed to examine and evaluate the equations for effective length factor K. These analyses and evaluations are presented in the sections that follow.

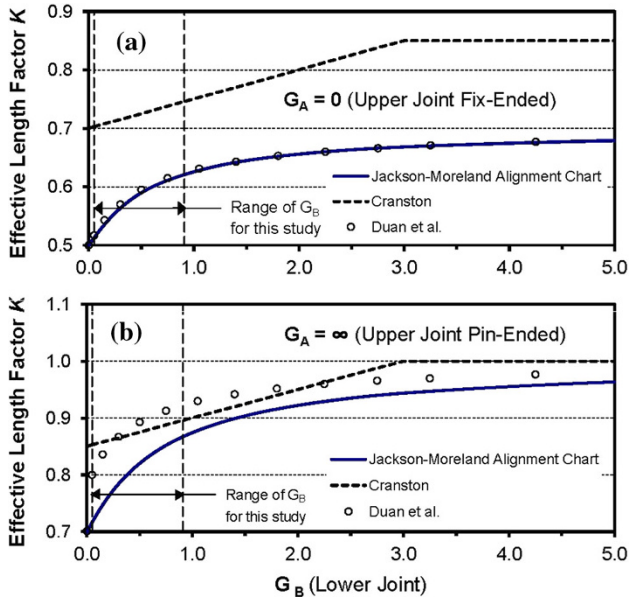

Fig. 9 Comparison of effective length factors (K) computed from different design equations when **a** the upper joint of the column is fix-ended; and **b** the upper joint of the column is pin-ended.

8. Examination of Computed Ultimate Strengths of Columns in Simulated Braced Frames

8.1 Overview of Strength Ratio Statistics

Only the columns where the theoretically-computed maximum magnified bending moment due to second-order effects along the height of the column was greater than the larger first-order end moment (M_2) were included in the analysis because for these columns δ_{ns} exceeds 1.0. As a result, the analysis presented here includes data for 2,168 of the 2,960 braced T-frames initially used for this study. Note that, for load cases 1, 2, 3 and 4, the first-order e/h ratios ($M_2/(P_{u(th)}h)$) ranged from 0.013 to 0.192 and M_2 was located at the bottom end of the column. For load cases 5 and 6 a full range of first-order e/h ratios ($M_2/(P_{u(th)}h)$) from 0.1 to 1.0 was used by applying M_2 to the top end of the column, which was pin-ended.

Histograms and statistics of column strength ratios ($P_{u(th)}/P_{u(des)}$) prepared from the combined data for load cases 1–4 are plotted in Fig. 10a, b and those prepared from the combined data for load cases 5 and 6 are shown in Fig. 10c, d. Note that Fig. 10c, d represent columns in frames for which an external bending moment was applied at the top end of the column in addition to the beam and column loads. For computing these strength ratios, $P_{u(des)}$ was calculated in four different ways by using δ_{ns} from Eq. (2) with the column effective length factor K computed from Eq. (5) (Jackson–Moreland Alignment Chart) or Eq. (8) (Duan et al. 1993) and the effective flexural stiffness EI computed from Eq. (4) (ACI) or Eq. (7) (Tikka and Mirza 2005). Hence, Fig. 10a, c were prepared using K computed from the Jackson–Moreland Alignment Chart, whereas Fig. 10b, d were plotted with K based on the Duan et al. equation. Note that strength ratios ($P_{u(th)}/P_{u(des)}$) greater than 1.0 signify that $P_{u(des)}$ is conservative and vice versa. Figure 10 leads to the following conclusions:

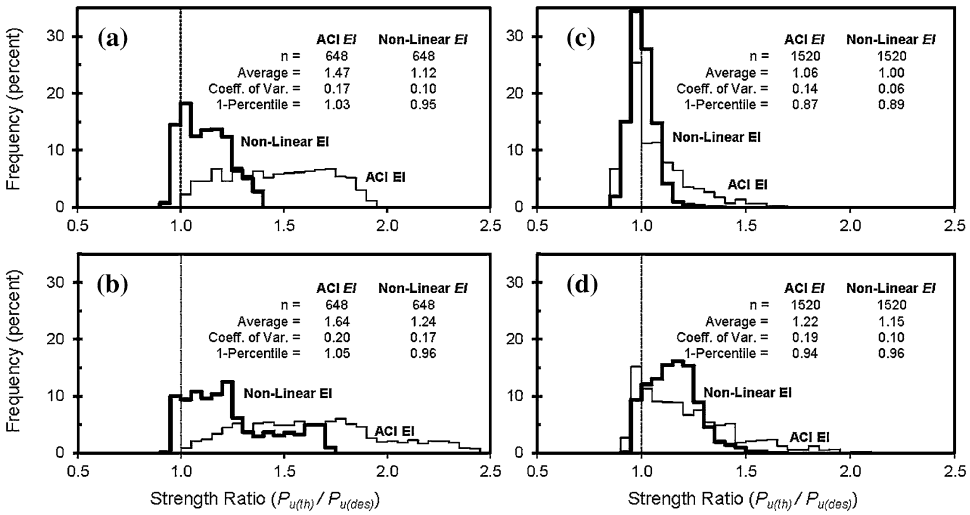

Fig. 10 Histograms for strength ratios calculated using ACI *EI* and nonlinear *EI* (Eqs. (4) and (7), respectively) for load cases 1, 2, 3 and 4: **a** *K* computed from Jackson–Moreland Alignment Chart and **b** *K* computed from Duan et al.; and for load cases 5 and 6: **c** *K* computed from Jackson–Moreland Alignment Chart and **d** *K* computed from Duan et al.

1. A comparison of Fig. 10a, b, both prepared for load cases 1–4, clearly demonstrates that the strength ratio statistics are more compact and the related histograms are tighter in Fig. 10a where *K* was computed from the Jackson–Moreland Alignment Chart than those in Fig. 10b where *K* was calculated from the Duan et al. equation. This is regardless of whether the ACI or nonlinear *EI* equation is used for computing P_c. These conclusions also appear valid when Fig. 10c, d plotted for load cases 5–6 are compared. Hence, there is no advantage in replacing the Jackson–Moreland Alignment Chart by the Duan et al. equation for the effective length factor *K* for the type of reinforced concrete frames studied.
2. A comparison of strength ratio statistics and related histograms in Fig. 10a indicates that the variability of the strength ratios decreases significantly and the histogram becomes much tighter when the nonlinear *EI* equation is used in place of the ACI *EI* equation for computing P_c. The same conclusion can be reached by examining the statistics and related histograms of Fig. 10b, c, or d. Hence, regardless of whether *K* is computed from the Jackson–Moreland Alignment Chart or from the Duan et al. equation and also regardless of whether load cases 1–4 or load cases 5–6 are examined, the nonlinear *EI* equation produces more accurate results than does the ACI *EI* equation. This is expected considering the fact that an earlier study by Tikka and Mirza (2005) has established that the nonlinear *EI* equation computes the strength of isolated reinforced concrete columns more accurately than does the ACI *EI* equation.
3. More compact statistics and tighter histograms were produced for load cases 5–6 ploted in Fig. 10c as opposed to those produced for load cases 1–4 and shown in Fig. 10a. The same conclusion can be drawn by comparing Fig. 10d for load cases 5–6 with Fig. 10b for load cases 1–4. However, in almost all cases, lower one-percentile strength ratios were produced for load cases 5–6 than for load cases 1–4. This is likely due to the fact that the external *e/h* ratios ranged from 0.1 to 1.0 for columns in load cases 5–6 compared to those ranging merely from 0.013 to 0.192 for columns in load cases 1–4.
4. The most compact statistics and related histograms are produced when, in computation of P_c, the effective length factor *K* is taken from the Jackson–Moreland Alignment Chart (Eq. (5)) and the effective flexural stiffness *EI* is based on the nonlinear equation (Eq. (7)) proposed by Tikka and Mirza (2005), as indicated by Fig. 10a plotted for load cases 1–4 and by Fig. 10c prepared for load cases 5–6.

8.2 Effects of Variables on Strength Ratios

For load cases 1, 2, 3 and 4, the end eccentricity ratio ($e/h = M_2/P_{u(th)}h$) ranges from 0.013 to 0.192 and the end moment ratio (M_1/M_2) is equal to -0.5 or 0.0 when the upper end of the column is fix-ended or pin-ended, respectively. Therefore, the effects of *e/h* and M_1/M_2 on the strength ratio ($P_{u(th)}/P_{u(des)}$) will not be shown for load cases 1–4, because no trends were readily visible in the ranges of *e/h* and M_1/M_2 studied. Furthermore, as the beam moment ratio ($M_{bm}/M_{y(bm)}$) displayed little effect on the strength ratios of columns in frames subjected to load cases 1–4 or to load cases 5–6 within the range of $M_{bm}/M_{y(bm)}$ studied (0.84–1.12), those plots will not be shown for any of the load cases.

The effect of column slenderness ratio ($K\ell/r$) on the column strength ratio is examined in Fig. 11. This figure was prepared for load cases 1–4 combined involving 648 reinforced concrete frames, where the theoretically-computed maximum magnified moment due to second-order effects

along the column height was greater than M_2. Note that, for computing the strength ratios shown in Fig. 11, $P_{u(des)}$ was determined in the same manner as for the histograms plotted in Fig. 10a, b using the ACI procedure for computing δ_{ns} (Eq. (2)) and one of the following four sets of equations for K and EI: (a) the effective length factor from Eq. (5) (Jackson–Moreland Alignment Chart) and EI from Eq. (4) (ACI) for Fig. 11a; (b) the effective length factor from Eq. (5) (Jackson–Moreland Alignment Chart) and EI from nonlinear Eq. (7) (Tikka and Mirza 2005) for Fig. 11b; (c) the effective length factor from Eq. (8) (Duan et al. 1993) and ACI EI from Eq. (4) for Fig. 11c; and (d) the effective length factor from Eq. (8) (Duan et al. 1993) and EI from nonlinear Eq. (7) (Tikka and Mirza) for Fig. 11d. Note that, for the ACI moment magnifier procedure, δ_{ns} was calculated from axial loads and bending moments obtained from the conventional (first-order) elastic frame analysis.

The strength ratios shown in Fig. 11 indicate that the four combinations of K and EI noted above produce safe designs for all $K\ell/r$ values studied including for those that are beyond the upper limit of 100 placed on $K\ell/r$ by the North American structural codes (ACI 2005 and CSA 2004). Figure 11 also leads to the following conclusions:

1. As stated earlier, Fig. 11a, b were plotted using K from the Jackson–Moreland Alignment Chart. Figure 11a shows that, when the ACI EI equation (Eq. (4)) is used, the strength ratios become increasingly conservative as $K\ell/r$ increases from approximately 40–110. Mirza (1990) suggests that this is perhaps because the cracks are likely to be more widely spaced in a longer column with more concrete in between the cracks contributing to the column stiffness, thereby leading to the conclusion that the ℓ/h ratio should be included as a variable in the column EI equation to capture this effect. However, the ACI EI equation does not include ℓ/h as a variable. A comparison of Fig. 11a with 11b shows that, when the nonlinear EI equation (Eq. (7)) is used, the effect of $K\ell/r$ on the strength ratios becomes insignificant. This is expected because ℓ/h is one of the variables used for the nonlinear EI equation.
2. Figure 11c, d were prepared from K based on the Duan et al. equation. A comparison of Fig. 11c with a, and that of Fig. 11d with b, shows that Fig. 11c, d produce more scattered strength ratios than Fig. 11a, b. This is expected because the Duan et al. equation computes more conservative values of K for pin-ended columns than those given by the Jackson–Moreland Alignment Chart, whereas both Jackson–Moreland Alignment Chart and Duan et al. equation compute very close values of K for fix-ended columns, as indicated by Fig. 9. Consequently, Fig. 11c, d show two distinct groups of data, one for fix-ended columns and the other for pin-ended columns. Hence, Fig. 11 reinforces an earlier conclusion that there appears to be no advantage in replacing the Jackson–Moreland Alignment Chart by the Duan et al. equation for the type of frames studied.
3. The strength ratios plotted in Fig. 11b are based on K computed from the Jackson–Moreland Alignment Chart (Eq. (5)) and EI calculated from the nonlinear equation (Eq. (7)). These strength ratios show the least scatter, the most compact statistics and the least effect of $K\ell/r$ when compared to Fig. 11a, c, and d.

The effects of e/h, M_1/M_2, and $K\ell/r$ on the strength ratios for the combined data from load cases 5 and 6 are shown in Figs. 12 and 13. These figures were plotted for 1,520 reinforced concrete frames, where the theoretically-computed maximum magnified moment due to second-order effects along the column height was greater than M_2. Consequently, as e/h increases from 0.1 to 1.0, the number of data points in Figs. 12 and 13 decreases from 220 at $e/h = 0.1$ to 132 at

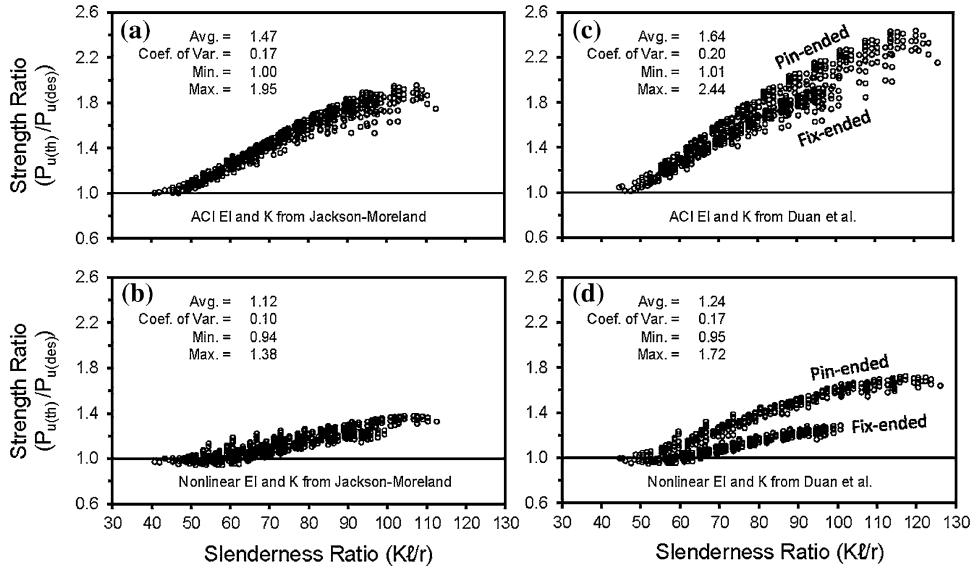

Fig. 11 Effect of column slenderness ratio on strength ratios for load cases 1, 2, 3 and 4 ($n = 648$) calculated using **a** K from Jackson–Moreland Alignment Chart and EI from ACI equation; **b** K from Jackson–Moreland Alignment Chart and EI from nonlinear equation; **c** K from Duan et al. and EI from ACI equation; and **d** K from Duan et al. and EI from nonlinear equation.

$e/h = 1.0$. Note that M_1/M_2 ratio in these figures ranges from -0.4 (double curvature bending, $C_m = 0.44$) to 1.0 (single curvature bending, $C_m = 1.0$). For computing the strength ratios shown in Figs. 12 and 13, $P_{u(des)}$ was determined in the same manner as for the histograms plotted in Fig. 10c, d using the ACI procedure for computing δ_{ns} (Eq. (2)) and one of the following four sets of equations for K and EI: (a) The effective length factor from Eq. (5) (Jackson–Moreland Alignment Chart) and ACI EI from Eq. (4) for Fig. 12a–c; (b) the effective length factor from Eq. (5) (Jackson–Moreland Alignment Chart) and nonlinear EI from Eq. (7) (Tikka and Mirza 2005) for Fig. 12d–f; (c) the effective length factor from Eq. (8) (Duan et al. 1993) and ACI EI from Eq. (4) for Fig. 13a–c; and (d) the effective length factor from Eq. (8) (Duan et al.) and nonlinear EI from Eq. (7) (Tikka and Mirza) for Fig. 13d–f.

The results shown in Fig. 12 for load cases 5 and 6 for which K was computed from Jackson–Moreland Alignment Chart lead to the following conclusions:

1. Figure 12 shows a very large spread in strength ratios when the ACI equation is used for computing EI (Eq. (4)). This is particularly valid for strength ratios with $e/h < 0.3$, $-0.3 < M_1/M_2 < 0.8$, and $K\ell/r > 70$, as indicated by Fig. 12a, b, and c, respectively.
2. A comparison of Fig. 12a, b, and c with d, e, and f, respectively, indicates that the spread in strength ratios reduces very significantly when the nonlinear EI equation (Eq. (7)) is used in lieu of the ACI EI equation (Eq. (4)). In fact, strength ratios shown in Fig. 12d–f appear to be almost independent of e/h, M_1/M_2, and $K\ell/r$ ratios, respectively. This is expected because e/h and ℓ/h are included as variables in the nonlinear EI equation.

The Duan et al. equation was employed in place of the Jackson–Moreland Alignment Chart to calculate the K factor used in $P_{u(des)}$ for computing the strength ratios from load cases 5 and 6 plotted in Fig. 13. The δ_{ns} and EI equations used in $P_{u(des)}$ for preparing Fig. 13 are identical to those for Fig. 12. This permitted an examination of the effect on strength ratios of using the Duan et al. equation for the K factor. A comparison of Figs. 13 with 12 shows a higher spread in strength ratios plotted in Fig. 13, where the Duan et al. equation (Eq. (8)) was used for computing K, as

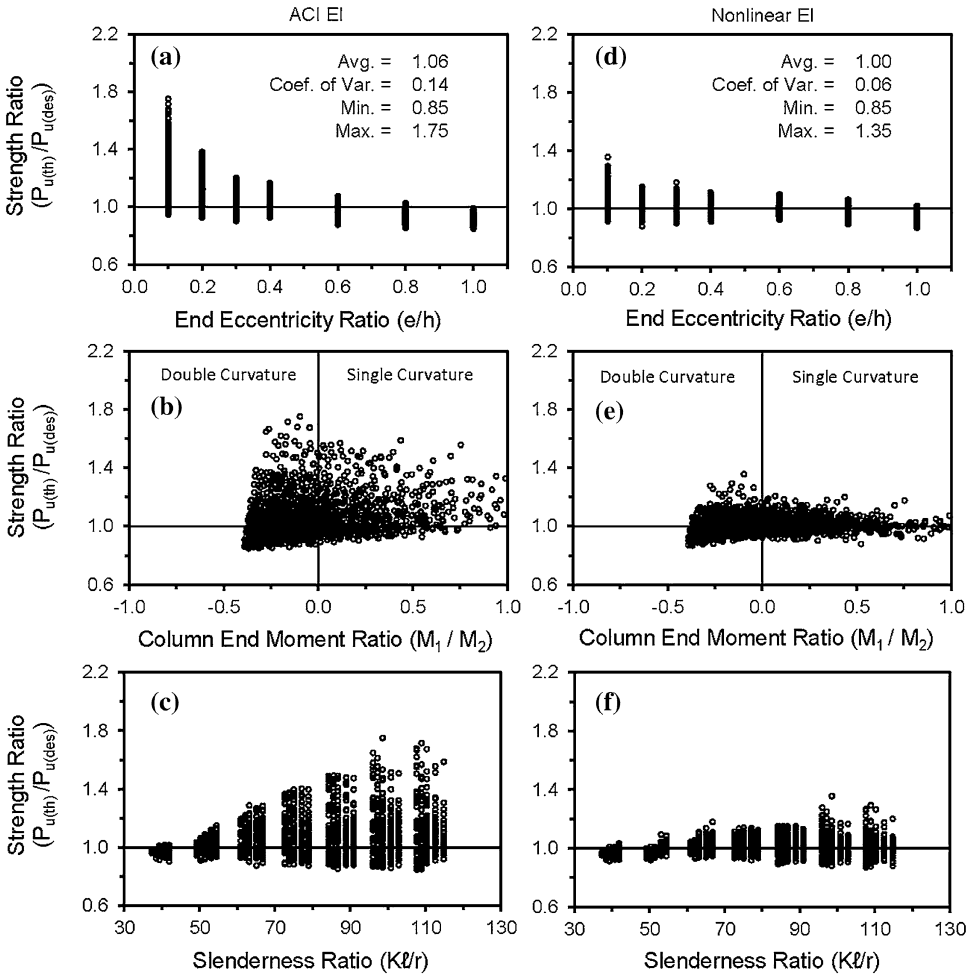

Fig. 12 Effects of variables on strength ratios for load cases 5 and 6 ($n = 1{,}520$) calculated using K from Jackson–Moreland Alignment Chart with EI from ACI equation: **a** end eccentricity ratio (e/h); **b** column end moment ratio (M_1/M_2); **c** slenderness ratio ($K\ell/r$); and with EI from nonlinear equation; **d** end eccentricity ratio (e/h); **e** column end moment ratio (M_1/M_2); **f** slenderness ratio ($K\ell/r$).

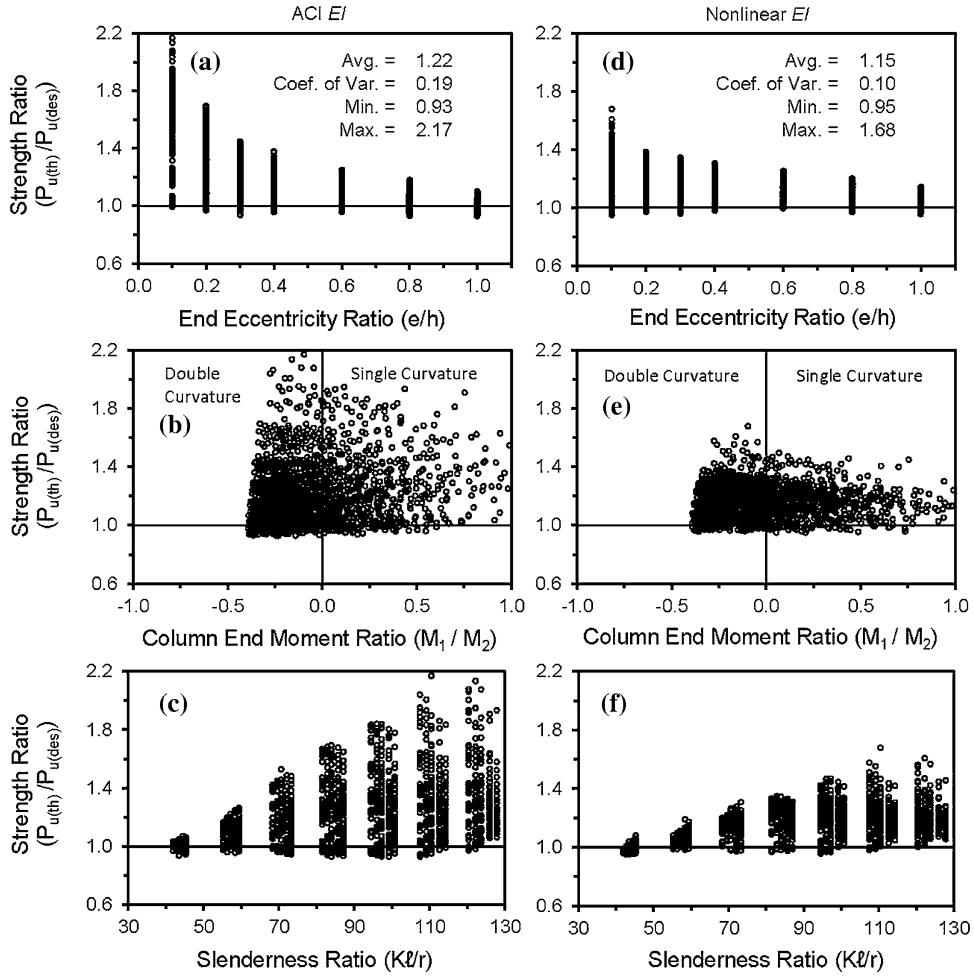

Fig. 13 Effects of variables on strength ratios for load cases 5 and 6 ($n = 1{,}520$) calculated using K from Duan et al. equation with EI from ACI equation: **a** end eccentricity ratio (e/h); **b** column end moment ratio (M_1/M_2), **c** slenderness ratio ($K\ell/r$); and with EI from nonlinear equation: **d** end eccentricity ratio (e/h); **e** column end moment ratio (M_1/M_2); **f** slenderness ratio ($K\ell/r$).

opposed to Fig. 12 where the Jackson–Moreland Alignment Chart (Eq. (5)) was employed for determining the K factor. This is irrespective of whether the ACI EI or nonlinear EI equation is used for computing $P_{u(des)}$. Again, this should be expected as explained earlier and indicates no advantage in replacing the Jackson–Moreland Alignment Chart with the Duan et al. equation for the types of frames studied. Furthermore, a comparison of all four sets of strength ratios plotted in Figs. 12 and 13 indicates that the strength ratios based on K from Jackson–Moreland Alignment Chart and EI from the nonlinear equation and shown in Fig. 12d–f demonstrate the least scatter, the most compact statistics, and practically no effect of e/h, M_1/M_2, and $K\ell/r$ over almost the entire ranges of these variables studied.

8.3 Strength Ratios for Individual Load Cases Produced Using K from Jackson–Moreland Alignment Chart and EI from Nonlinear Equation

It is evident from Figs. 10, 11, 12, and 13 that the least variable strength ratios ($P_{u(th)}/P_{u(des)}$) are obtained when $P_{u(des)}$ is computed from Jackson–Moreland Alignment Chart for K (Eq. (5)) and the nonlinear equation for EI (Eq. (7)) proposed by Tikka and Mirza (2005). The accuracy of $P_{u(des)}$ based on these equations for K and EI was further examined from histograms and related statistics of strength ratios prepared for load cases 1–6 individually. Figure 14 shows resulting histograms and statistics with average strength ratios, coefficients of variation, and one-percentile values ranging from 1.07 to 1.18, 0.07 to 0.11, and 0.94 to 1.00, respectively, for load cases 1–4 and from 1.00 to 1.01, 0.05 to 0.07, and 0.88 to 0.90, respectively, for load cases 5–6. These statistics and histograms indicate low and more than acceptable variations in strength ratios when $P_{u(des)}$ is based on K from Jackson–Moreland alignment Chart and EI from the nonlinear equation proposed by Tikka and Mirza (2005). It is, therefore, suggested that the nonlinear equation for EI should be permitted, but not required, by ACI 318. This would allow structural engineers the use of an equation with better design precision when desired.

9. Summary and Conclusions

The ACI 318-11 permits the use of the moment magnifier method for computing the ultimate strength of a slender reinforced concrete column. This computed ACI strength is

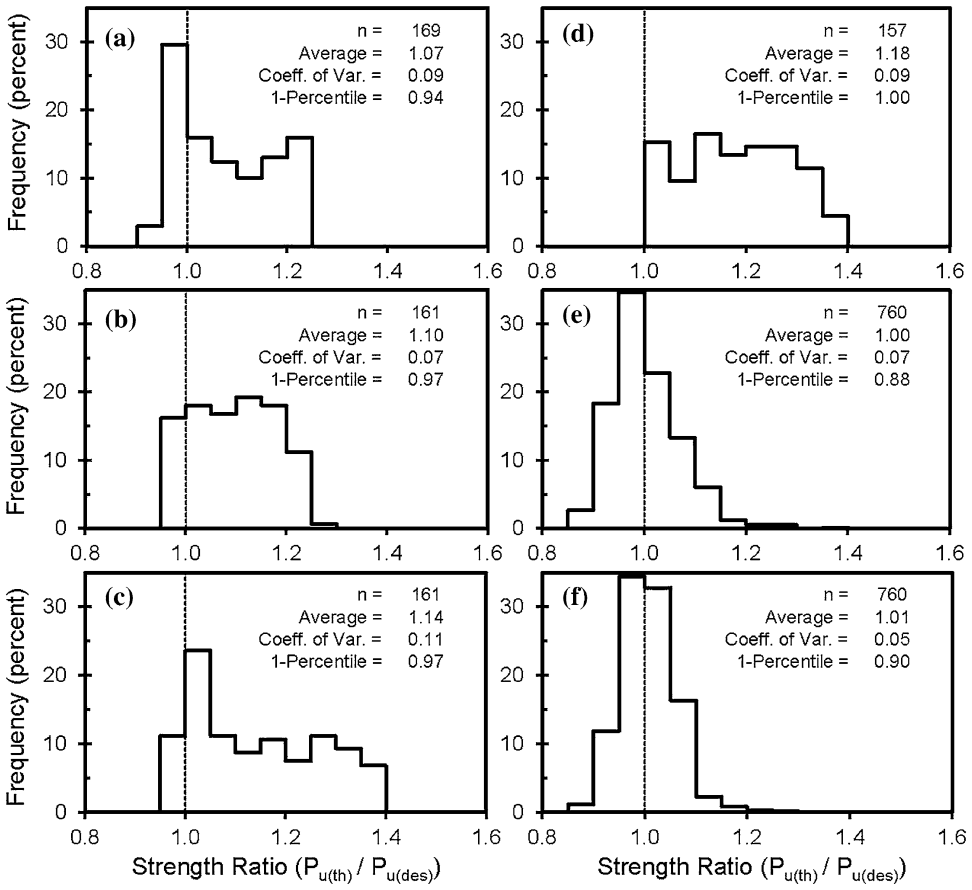

Fig. 14 Histograms for strength ratios calculated using K from Jackson–Moreland Alignment Chart and EI from nonlinear equation: **a** load case (1); **b** load case (2); **c** load case (3); **d** load case (4); **e** load case (5); and **f** load case (6).

influenced by the column effective length factor K and the effective flexural stiffness EI among other factors. For this study, 2,960 reinforced concrete braced frames in the shape of an inverted T subjected to short term loads were simulated to evaluate the accuracy of equations for K. An elaborate theoretical strength model was developed and used for computing the ultimate strengths of columns in simulated frames. The theoretically computed column ultimate strengths were divided by the strengths of the same columns calculated from the ACI moment magnifier method using different combinations of K and EI equations to obtain the nondimensionalized strength ratios. The strength ratios were then statistically analyzed to evaluate the accuracy of K equations investigated. The strength and stiffness reduction factors were taken equal to 1.0 for computing the ACI ultimate strengths.

From the results presented in this paper, it is concluded that (a) there is no advantage in replacing the Jackson–Moreland Alignment Chart with equations available in the literature for computing the K factor; and (b) the computational accuracy of the moment magnifier method can be significantly improved by replacing the ACI EI equation with the nonlinear EI equation proposed by Tikka and Mirza. Hence, the ACI ultimate strength can be most accurately computed from the moment magnifier method when the effective length factor K is computed using the Jackson–Moreland Alignment Chart and by adopting a nonlinear equation for computing EI proposed for design by Tikka and Mirza. It is suggested that ACI 318 should permit the use of the EI equation proposed by Tikka and Mirza.

Open Access

References

ACI Committee 318. (2005). *Building code requirements for structural concrete (ACI 318-05) and commentary (ACI 318R-05)*. Farmington Hills, MI: American Concrete Institute.

ACI Committee 318. (2011). *Building code requirements for structural concrete (ACI 318-11) and commentary.* Farmington Hills, MI: American Concrete Institute.

Bazant, Z. P., & Oh, B. H. (1984). Deformation of progressively cracking reinforced concrete beams. *ACI Journal, 81*(3), 268–278.

Blomeier, G. A., & Breen, J. E. (1975). Effect of yielding of restraints on slender concrete columns with sidesway

prevented. In *Reinforced concrete columns, SP-50* (pp. 41–65). Detroit, MI: American Concrete Institute.

Breen, J. E., & Ferguson, P. M. (1964). The restrained long concrete column as a part of a rectangular frame. *ACI Journal, 61*(5), 563–587.

CAC. (2006). *Explanatory notes on CSA standard A23.3-04. Concrete design handbook* (3rd ed.) (pp. 217–358). Ottawa, ON: Cement Association of Canada.

Chen, W. F., & Lui, E. M. (1987). *Structural stability—Theory and implementation*. New York, NY: Elsevier Science Publishing Company Inc.

Cranston, W. B. (1972). Analysis and design of reinforced concrete columns. Research Report No. 20, Paper 41.020, Cement and Concrete Association, London, England.

CSA. (2004). *Design of concrete structures—CSA standard A23.3-04*. Mississauga, ON: Canadian Standard Association.

Duan, L., King, W. S., & Chen, W. F. (1993). *K*-factor equation to alignment charts for column design. *ACI Structural Journal, 90*(3), 242–248.

Ford, J. S., Chang, D. C., & Breen, J. E. (1981a). Experimental and analytical modeling of unbraced multipanel concrete frames. *ACI Journal, 78*(1), 21–35.

Ford, J. S., Chang, D. C., & Breen, J. E. (1981b). Behavior of unbraced multipanel concrete frames. *ACI Journal, 78*(2), 97–115.

Ford, J. S., Chang, D. C., & Breen, J. E. (1981c). Design indications from tests of unbraced multipanel concrete frames. *Concrete International, 3*(3), 37–47.

Furlong, R. W., & Ferguson, P. M. (1966). Test of frames with columns in single curvature. In *Symposium on reinforced concrete columns, SP-13* (pp. 55–73). Detroit, MI: American Concrete Institute.

Mirza, S. A. (1990). Flexural stiffness of rectangular reinforced concrete columns. *ACI Structural Journal, 87*(4), 425–435.

Mirza, S. A., & MacGregor, J. G. (1989). Slenderness and strength reliability of reinforced concrete columns. *ACI Structural Journal, 86*(4), 428–438.

Park, R., Priestly, M. J. N., & Gill, W. D. (1982). Ductility of square-confined concrete columns. *Journal of the Structural Division, ASCE, 108*(ST4), 929–950.

Tikka, T. K., & Mirza, S. A. (2002). Examination of second-order effects in structural concrete columns and braced frames. Civil Engineering Research Series Report No. CE-02-2, Lakehead University, Thunder Bay, ONtario, Canada.

Tikka, T. K., & Mirza, S. A. (2004). Equivalent uniform moment diagram factor for reinforced concrete columns. *ACI Structural Journal, 101*(4), 521–531.

Tikka, T. K., & Mirza, S. A. (2005). Nonlinear *EI* equation for slender reinforced concrete columns. *ACI Structural Journal, 102*(6), 839–848.

Yalcin, C., & Saatcioglu, M. (2000). Inelastic analysis of reinforced concrete columns. *Computers & Structures, 77*(5), 539–555.